Available online at www.sciencedirect.com
ScienceDirect
Journal of the European Ceramic Society 31 (2011) 1219–1225
www.elsevier.com/locate/jeurceramsoc

Creep behavior and related structural defects in Al_2O_3–Ln_2O_3 (ZrO_2) directionally solidified eutectics (Ln = Gd, Er, Y)

L. Mazerolles [a,*], L. Perriere [a,b], S. Lartigue-Korinek [a], M. Parlier [b]

[a] *Institut de Chimie et des Matériaux Paris-Est, UMR 7182/CNRS-Paris 12, 2-8 rue Henri Dunant 94407 Thiais, France*
[b] *Office National d'Etudes et de Recherches Aérospatiales, 92322 Châtillon, France*

Available online 21 August 2010

Abstract

The eutectic architecture of "in situ" composites prepared by solidification from the melt in the Al_2O_3–Ln_2O_3 (ZrO_2) systems gives rise to materials with a high creep resistance. With the objective to elucidate the high temperature deformation micro-mechanisms, microstructural features are investigated on crept specimens. Compressive creep experiments have been carried out between 1400 and 1550 °C for various eutectic compositions. Different deformation regimes depending on considered systems and conditions of stress and temperature are revealed. Transmission electron microscopy studies emphasize the activation of different slip systems in the alumina phase and the deformation by dislocation climb processes controlled by bulk diffusion.

Keywords: Defects; Electron microscopy; Creep; Al_2O_3; Eutectics

1. Introduction

The development of new ultra-high temperature structural materials in various fields such as gas turbine or thermal power generation systems is required to improve energy efficiency and also to reduce polluting emission of CO_2 or NO_x. For example, the Ni-based superalloys, currently used for making single-crystal turbine blades operating in motors, will not be able to work at temperatures beyond 1150 °C, despite research activities for increasing their heat resistance. Besides, oxidation mechanisms that occur at high temperatures (>1300 °C) also limit the use of ceramic matrix composites consisting of silicon carbide fibers – or whiskers – embedded in a ceramic matrix. Melt growth composites (MGC) of oxides prepared at eutectic composition appear to be promising materials by coupling single-crystal phases within a microstructure almost free of grain boundaries in addition to their intrinsic resistance to oxidation. These ceramic materials prepared by unidirectional solidification from the melt add new potentialities compared to sintered ceramics: a high strength almost constant up to temperatures close to the melting point (no secondary phase at the grain boundaries), a stable microstructure and no chemical reaction between the component phases.[1–5] However, these composites being grown from the melt, a large thermal expansion mismatch between the eutectic phases and the anisotropy of microstructure can be often seen as major drawbacks because they give rise to cracks inside the material during cooling. In the last 10 years, studies on eutectic compositions in the Al_2O_3–Ln_2O_3 systems, have given rise to synthesis of "in situ" composites displaying microstructures consisting of two entangled phases in a three-dimensional and continuous network. This novel family of directionally solidified eutectic ceramics present outstanding mechanical properties as a flexural strength constant up to temperatures close to T_m and a good creep resistance.[6–11] Extension to ternary systems, by addition of zirconia for improving fracture toughness was also achieved.[12–14]

The aim of the present work is to understand the mechanisms that control creep behavior of these materials at high temperatures (1400–1600 °C). In this purpose, specimens were prepared from various Al_2O_3–Ln_2O_3 systems and crept using compressive tests. Transmission electron microscopy studies were performed on thin foils extracted from deformed specimen. All the used methods are described in the experimental procedure. The first part of the results describes the overall microstructural features of as-processed specimens. The creep behavior and macroscopic deformation parameters are detailed in a second part. The last part of this paper presents the defect analyses at a microscopic scale. Detailed investigations of dislocation

* Corresponding author.
E-mail address: mazerolles@glvt-cnrs.fr (L. Mazerolles).

0955-2219/$ – see front matter © 2010 Elsevier Ltd. All rights reserved.
doi:10.1016/j.jeurceramsoc.2010.07.040

Table 1
Chemical compositions and constituent phases of studied eutectics.

Composition (mol.%)	Eutectic phases	Structure of phases
$77Al_2O_3$–$23Y_2O_3$	Al_2O_3–$Y_3Al_5AlO_{12}$	Corundum (trigonal)
$81Al_2O_3$–$19Er_2O_3$	Al_2O_3–$Er_3Al_5AlO_{12}$	+ garnet (cub.)
$77Al_2O_3$–$23Gd_2O_3$	Al_2O_3–$GdAlO_3$	corundum (trigonal) + perovskite (ortho.)
$65Al_2O_3$–$16Y_2O_3$–$19ZrO_2$	Al_2O_3–$Y_3Al_5AlO_{12}$–ZrO_2	corundum (trigonal)
$66Al_2O_3$–$15.5Er_2O_3$–$18.5ZrO_2$	Al_2O_3–$Er_3Al_5AlO_{12}$–ZrO_2	+ garnet (cub.) + fluorite (cub.)
$58Al_2O_3$–$19Gd_2O_3$–$23ZrO_2$	Al_2O_3–$GdAlO_3$–ZrO_2	Corundum (trigonal) + perovskite (ortho.) + fluorite (cub.)

configurations have been mainly performed in alumina phase that presents various slip systems with different stress and temperature dependence. We show that creep mechanisms depend on the macroscopic thermomechanical loading (temperature, stress) and are related to the microstructural characteristics.

2. Experimental procedure

The oxide–oxide eutectics were grown from the melt by using a floating zone translation device consisting in an arc-image furnace operating with a 6 kW xenon lamp as a radiation. The great interest of this equipment is to display high thermal gradients in the solidification direction that are required for planar front growth conditions.[15] Solidification was driven in air at a constant speed ranging from 2 to 20 mm h^{-1}. As-prepared specimen display a cylindrical symmetry and dimensions of about 8 mm in diameter and 50 mm in length. Creep tests reported in this paper were performed on eutectic compositions solidified at a 10 mm h^{-1} solidification rate.

High-purity commercial powders (99.9%) were used for starting materials. They were mixed at eutectic composition, pressed in cylinder bars and consolidated by sintering at 1400 °C before melting.

Specimen for creep experiments, were machined from the solidified eutectic bars with dimensions of $2.5 \times 2.5 \times 5\ mm^3$. Tests were performed in compression (the uniaxial applied stress being parallel to the solidification direction), in air environment with a temperature range 1450–1600 °C. The sample was put under stress by dead-weight loading. Stress ranges from 70 to 200 MPa. Compression rams were made of sintered alumina bars coupled with sapphire rods oriented along the *c*-axis. Platens cut perpendicularly to the axis of solidified eutectic bars were sandwiched between these sapphire rods and the specimen. Temperature was measured with two sets of B-type thermocouples located in the furnace and in the near vicinity of the specimen. Strains, during the creep tests were calculated from extensometric displacements measured using a linear transducer.

Microstructural studies were performed by scanning electron microscopy (SEM) (LEO1530) and transmission electron microscopy (TEM) (JEOL 2000EX). TEM foils were cut perpendicularly to the compressive axis and prepared by ion-milling after mechanical polishing and dimpling.

3. Results and discussion

3.1. Microstructures and crystallography

The as-prepared eutectic compositions, are summarized in Table 1. Binary eutectics, display very similar microstructural features (morphology, homogeneity) which were previously reported[15,16] and some of them are recalled in Fig. 1. SEM observations performed on sections perpendicular or parallel to the growth axis, for each eutectic composition, did not reveal any difference between the two directions and confirmed the 3D isotropic features of the microstructure.[16] Only the microstructure corresponding to specimens prepared from the Al_2O_3–Y_2O_3 phase diagram exhibits a slightly larger domain mean size (Fig. 1a). The eutectic phases corresponding to the

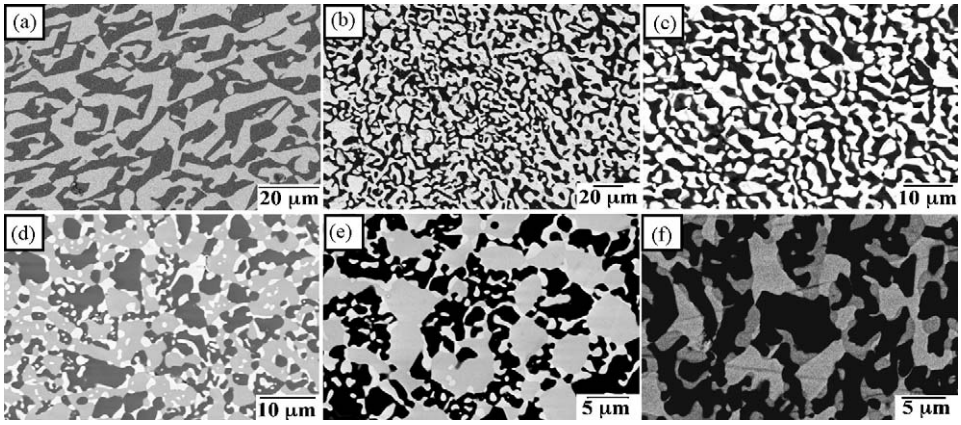

Fig. 1. SEM images of eutectic microstructures (BSE contrast). (a) Al_2O_3–Y_2O_3, (b) Al_2O_3–Er_2O_3, (c) Al_2O_3–G_2O_3, (d) Al_2O_3–Y_2O_3–ZrO_2, (e) Al_2O_3–Er_2O_3–ZrO_2, and (f) Al_2O_3–Gd_2O_3–ZrO_2. The dark contrast corresponds to the alumina phase. Zirconia phase corresponds to the white contrast for images d and e, and to the dark grey contrast in the image f.

Al_2O_3–Gd_2O_3 system were identified as Al_2O_3 (corundum structure) and $GdAlO_3$ (perovskite structure) named "GAP" afterwards. In the case of Al_2O_3–Y_2O_3 and Al_2O_3–Er_2O_3 systems the alumina phase is coupled to a Y (or Er)$_3Al_5O_{12}$ phase with a garnet structure called YAG (or EAG). The addition of ZrO_2 to these systems, at a ternary eutectic composition, has been shown to improve the fracture toughness of the Al_2O_3–Ln_2O_3 eutectics.[15] For comparison with binary systems, creep behaviors of three ternary eutectic compositions were also investigated. The microstructures of Al_2O_3–Ln_2O_3–ZrO_2 eutectics consist in two entangled phases with a zirconia phase located at the interfaces between alumina and the garnet (or perovskite) phase (Fig. 1d–f).

Unidirectional solidification process often imposes preferred crystallographic growth directions for each eutectic phase.[17,18] These directions and the crystallographic orientation relationships between phases, for the studied systems, were previously reported.[16] Orientations of specimen before creep were controlled, on large areas ($150 \times 150\ \mu m^2$), by EBSD spectroscopy and were also locally verified by TEM on transverse section platelets examined after creep.[16] The microstructures investigated in this paper were grown along the $\langle 1\,0\,\bar{1}\,0\rangle$ direction of alumina phase. Consequently, this orientation will be parallel to the compressive axis for the creep tests.

3.2. Compressive creep behavior

The creep deformation curves start by a primary transient creep regime during which the creep rate decreases in time. After this short primary stage (e.g. strain of about 0.5%) the quasi-steady state is reached with a quasi-constant creep rate. Then, in the course of the same experiment, the applied stress is changed, and primary and secondary creep rates are again measured for this new stress value. The strain rate strain plot in Fig. 2, for the Al_2O_3–YAG eutectic crept at 1525 °C, shows the quasi-steady state reached at different stress levels. The applied stress values were 70, 100, 140 and 200 MPa. Similar tests were performed under constant stress by temperature increments from 1440 to

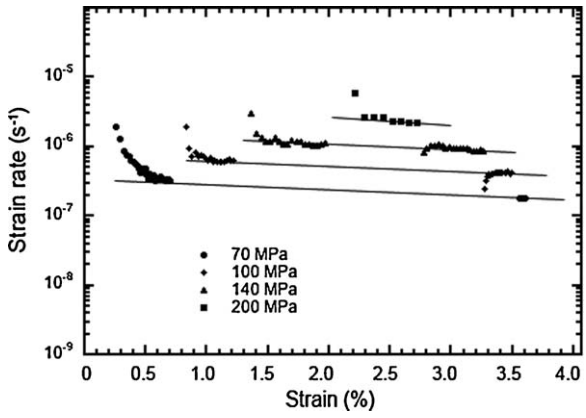

Fig. 2. Al_2O_3–YAG eutectic: typical strain rate strain plot, at different stress levels as loading and unloading cycles at 1525 °C.

1600 °C. The secondary creep rate, $\dot{\varepsilon}$, depends on the applied stress σ by a power–law relationship:

$$\dot{\varepsilon} = A \cdot \sigma^n \cdot \exp\left(\frac{-Q}{RT}\right)$$

where Q, proportional to the slope of the $\ln \dot{\varepsilon}$ vs. $1/T$ plot, is the apparent activation energy of creep.

The stress exponent, n, and the activation energy, Q, will be given by

$$n = \left(\frac{\partial \ln(\dot{\varepsilon})}{\partial \ln(\sigma)}\right)_T \quad Q = \left(\frac{\partial \ln(\dot{\varepsilon})}{\partial \ln(1/T)}\right)_\sigma$$

Consequently, tests performed at a given temperature (or stress) with load (or temperature) increments or decrements allow the determination of n and Q, respectively. Apparent activation energies for creep deformation are measured from the slope of semi-logarithmic Arrhenius plots of creep rate vs. inverse absolute temperature.

The stress dependence of creep strain rates at 1450 and 1525 °C (Fig. 3a) is very similar for the Al_2O_3–YAG and Al_2O_3–EAG eutectics. The stress exponent n increases with the stress at 1450 °C and is nearly constant at 1525 °C. At 1450 °C,

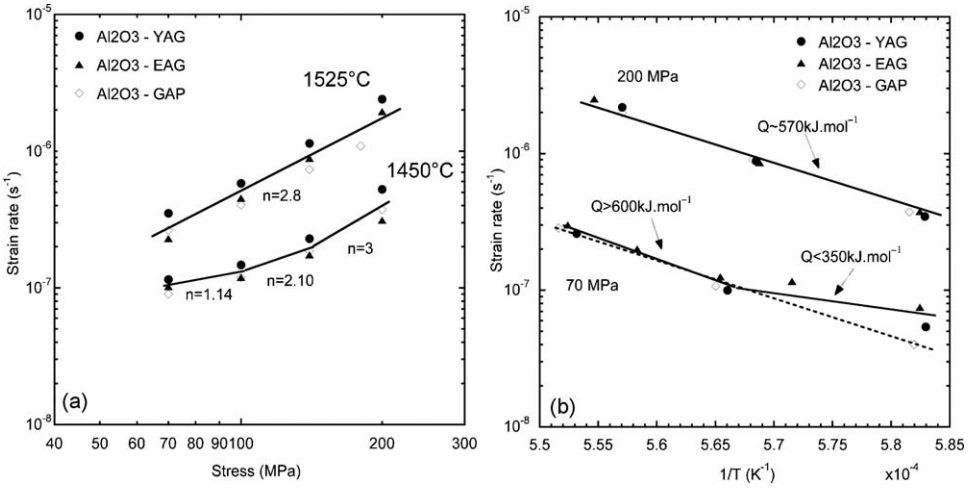

Fig. 3. Compressive creep test for the binary eutectics. (a) Creep strain rate vs. applied stress at 1450 and 1525 °C. (b) Creep strain rate vs. temperature ($1/T$) under 70 and 200 MPa loadings.

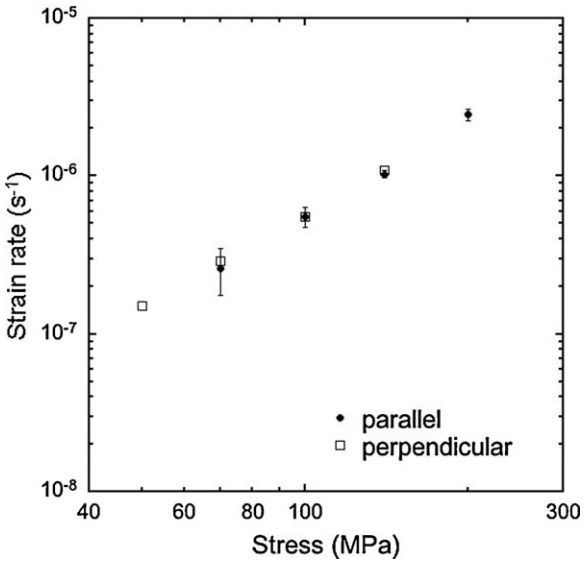

Fig. 4. Al_2O_3–YAG eutectic: comparison of strain rates at 1525 °C for compressive creep tests performed along the directions parallel and perpendicular to the growth direction.

the n values are close to 1, for low stresses, that suggests a diffusion-controlled creep mechanism. The n values are higher ($2 < n < 3$) in the case of high stress and/or high temperature: this could indicate deformation mechanisms controlled by dislocation motion. Variations of the activation energy (Fig. 3b) are very similar for the two eutectic compositions coupling alumina and garnet-type phase. For low applied stresses (70 MPa) the Q value is equal to 350 kJ mol^{-1} at temperatures lower than 1490 °C, and increases up to 600 kJ mol^{-1} above 1490 °C. This latter value is also observed for specimen crept under 200 MPa, on all over the temperature range. Similar values were also reported in literature.[19] Creep experiments performed with the compressive axis perpendicular to the growth direction did not reveal any difference. For example, Fig. 4 shows the creep results corresponding to the Al_2O_3–YAG composition with the stress applied along the direction parallel or perpendicular to the solidification axis ($T = 1525$ °C).

In the case of the Al_2O_3–GAP eutectic, the creep rates, measured with the same experimental conditions than previously, are on the same order of magnitude than that of eutectics coupling alumina and garnet type phases. However, the temperature incremental experiments do not reveal any regime change, and the activation energy is constant whatever the applied stress ($Q = 565$ kJ mol^{-1}).

Maximum strains ranging 10–15% (Al_2O_3–YAG) were reached under 200 MPa. Fig. 5 shows, that, beyond these strain values, the strain rate lightly increases, revealing the first damage steps of the specimen and the loss of the quasi-steady state. These strain values do not change with the studied binary system.

These results show that the orientation of specimen and the crystallographic form of the eutectic phase grown with the alumina phase (garnet or perovskite) do not really modify the creep rates of the eutectics. Besides, the deformation mechanisms probably differ, depending on temperature or stress range. The fact that the stress exponent, n, does not vary when the rare-

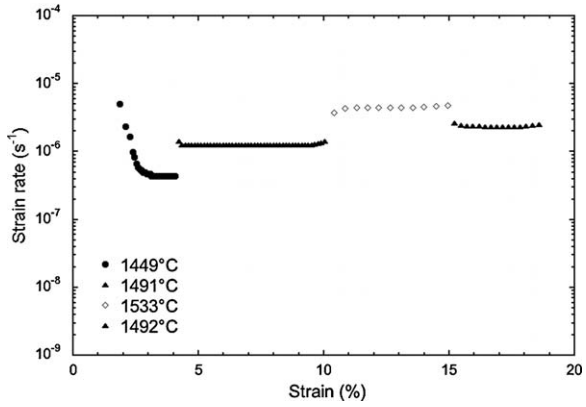

Fig. 5. Maximum strains obtained under 200 MPa for the Al_2O_3–YAG eutectic.

earth oxide rich phase coupled to alumina changes, suggests that plastic deformation is controlled by the α-alumina phase: a first regime sets up at low temperature ($T < 1500$ °C) and low stress then, a second regime occurs at higher temperatures and/or high stresses. The activation energy values confirm the hypothesis of two deformation regimes, with one of them preponderant depending on temperature and stress conditions.

The creep tests performed on ternary eutectics reveal strain rates with the same order of magnitude than that of their binary counterparts (Fig. 6). However, at the contrary of binary eutectics, the creep rates measured at 1525 °C for the Al_2O_3–GAP–ZrO_2 eutectic are higher than that of the Al_2O_3–YAG–ZrO_2 eutectic, and the inverse phenomena is observed at 1450 °C. This difference could be explained by the decrease of the microstructure mean size in the case of the Al_2O_3–YAG–ZrO_2 compared to the Al_2O_3–YAG eutectic. Experiments carried out under low stress (70 MPa) also reveal that the strain regime changes at 1500 °C in the case of the Al_2O_3–Al_2O_3–YAG–ZrO_2 eutectic. No change, on all over the temperature range, is observed for the Al_2O_3–GAP–ZrO_2 eutec-

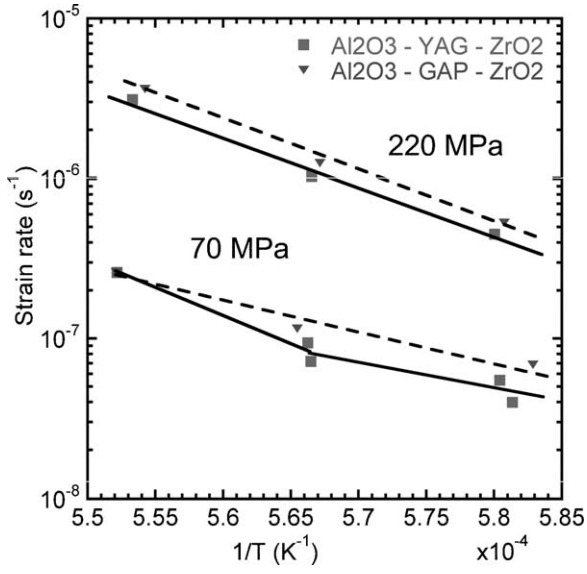

Fig. 6. Compressive creep test for the ternary eutectics. Creep strain rate vs. temperature ($1/T$) under 70 and 200 MPa loadings.

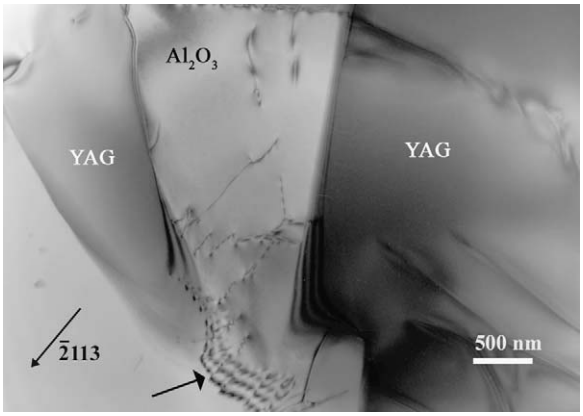

Fig. 7. Al_2O_3–YAG eutectic crept under 200 MPa (stress increments) at 1450 °C. Bright field image showing a network of dislocations with basal Burgers vectors in alumina, present at the thin extremity of a YAG phase (arrowed). Some dislocations appear in the YAG phase at the right of the micrograph.

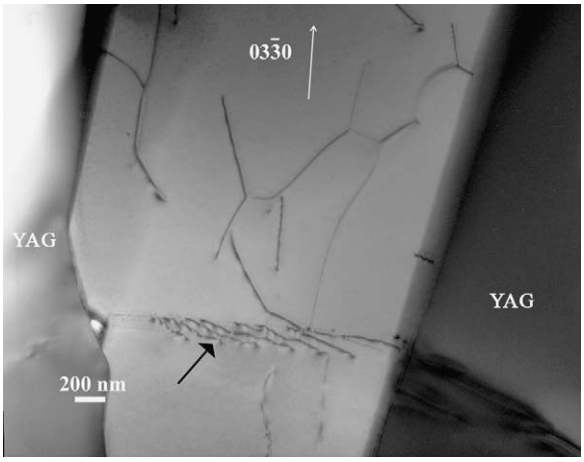

Fig. 8. Al_2O_3–YAG eutectic crept under 200 MPa (stress increments) at 1450 °C. Bright field image centred on an alumina crystal. A basal growth twin (horizontal, arrowed) contains extrinsic dislocations. Dislocations also appear in the YAG phases, on each side of the twin. A hole occurs at a triple junction. The coarse dislocation network present in alumina contains both basal and rhombohedral $1/3\langle 1\,0\,\bar{1}\,1\rangle$ dislocations.

tic. This behavior, similar to that of binary eutectics, confirms the influence of the garnet or the perovskite phase on the deformation mechanisms of the ternary or binary eutectic compositions. However, damage of specimen is reached more quickly during the creep tests with strains lower than that of binary eutectics (3–4%).

3.3. TEM study and discussion

Plastic deformation of single-crystal Al_2O_3 has been of interest for many years.[20,21] The two main slip systems are basal slip $(0\,0\,0\,1)1/3\langle 2\,\bar{1}\,\bar{1}\,0\rangle$, and prism plane slip $\{1\,1\,\bar{2}\,0\}\langle 1\,0\,\bar{1}\,0\rangle$. A non-extensive list of works on sapphire deformation may be found in Refs.[21–23] Basal slip has the lowest critical resolved shear stress at all temperatures above 700 °C.[23–25] Prism plane slip is preferred at lower temperature; at high temperature it occurs for much higher stresses than those required for basal glide[22] and prism plane dislocations are found to decompose into basal dislocations; prism plane dislocations are no more found after some percents of deformation.[22] Pyramidal slip $\{0\,1\,\bar{1}\,2\}1/3\langle 0\,\bar{1}\,1\,1\rangle$, or $\{1\,0\,\bar{1}\,1\}1/3\langle 0\,\bar{1}\,1\,1\rangle$, requires such high stresses that is rarely a dominant deformation mechanism. Rhombohedral dislocations are most often involved in processes other than those involving plastic deformation.[21] However, it is necessary to activate pyramidal slip if a homogeneous deformation is to be achieved by glide alone.[20] As the applied stress is parallel to $\langle 1\,0\,\bar{1}\,0\rangle$, the Schmid factor for basal glide is equal to 0.

Preliminary investigations have been performed on Al_2O_3–YAG eutectics deformed at 1450 °C under 200 MPa (after stress increments) and deformed at 1470 °C at a lower stress of 70 MPa. Some results previously obtained on an Al_2O_3–GAP eutectic are compared to the present analyses.[16]

Fig. 7 shows a bright field TEM image obtained on a thin foil of Al_2O_3–YAG eutectic after 1.5% deformation under compressive creep test at 1450 °C under 200 MPa. Dislocation networks are mainly observed in the alumina phase, and more particularly located in the narrow regions of the microstructure between two YAG domains. Analyses of other areas confirm that dislocation density is much lower in the YAG phase. As a matter of fact, YAG shows a ductile behavior for temperatures higher than 1600 °C, characterized by a dislocation climb controlled creep at very low strain rates.[26] These results show that the first steps of plastic deformation at this temperature, are controlled by the alumina phase, and the YAG phase accommodates this deformation. Such mechanism agrees well with the temperature dependence of the strain rate of Al_2O_3 which is higher, by several orders of magnitude, than that of YAG for the same solicitation direction.[27]

The dislocation network shown in Fig. 7 consists of basal dislocations with Burgers vectors of $1/3\langle 2\,\bar{1}\,\bar{1}\,0\rangle$ type. Their arrangement involves climb processes. It is recalled that the applied stress is parallel to the $(0\,0\,0\,1)$ basal plane; however, a slight angle of 3 degrees between the applied stress and the basal plane is sufficient to activate slip. It is also worth noticing that dislocations in alumina preferentially occurs at the edge of thin parts of the YAG phase, or near changes in orientation of the interface between the two phases, or in connections with dislocations in the other phase (see below). The YAG phase can thus be seen at the origin of stress concentrations that induce basal slip in alumina. It is worth noting that triaxial stresses help dislocation climb and orientate bulk diffusion.

Fig. 8 shows a coarse dislocation arrangement and isolated dislocations. A basal twin, that results from a growth accident during solidification,[16] contains extrinsic dislocations. Many interesting features, characteristic of the deformed microstructure, can be emphasized: dislocations occur in the YAG phase, close to the junction with the growth twin. Moreover, a hole is present at one of the triple junctions. The dislocation array contains both rhombohedral and basal dislocations. Three different rhombohedral dislocations are present, most of the Burgers vectors are not contained in the plane of the network. A possible reaction between the defects is as follows:

$$1/3[\bar{1}\,1\,0\,1] + 1/3[1\,\bar{2}\,1\,0] \Rightarrow 1/3[0\,\bar{1}\,1\,1]$$

This result leads to two conclusions. At first, the pyramidal slip has been activated, as a result of high local stress concentrations. Then, deformation proceeds with formation of networks with low energy configurations: this requires diffusion accommodated climb processes.

The Al_2O_3–YAG eutectic deformed at a similar temperature but under a low applied stress (70 MPa) displays a quite different microstructure characterised by much more less dislocations and the presence of basal deformation microtwins in alumina and planar defects in the YAG phase.

Finally, the Al_2O_3–GAP eutectic shows the presence of dislocations in both phases, as expected from the close temperature dependence of the most favoured dislocation slip systems in both phases.[16]

The lack of well defined slip planes or slip bands, the presence of dislocation nodes and configurations showing extensive climb are consistent with a deformation by dislocation climb controlled by bulk diffusion. The dislocation network consists of both basal and non-basal dislocations. In this view, some primary creep resulting from glide must also occur prior the formation of the stable dislocation network.[28] However, such primary creep is of short duration, as pyramidal slip requires very high stresses. This assumption is in good agreement with the activation energy values measured at 1500 °C (668 kJ/mol). Indeed this activation energy is of the same order of magnitude of oxygen bulk diffusion.[29,30]

The microtwins could occur as an accommodation mechanism of a deformation controlled by diffusion. Much more work is needed to improve the knowledge of deformation mechanisms and in particular the role of heterophase interfaces in defect formation, in agreement with the fact that macroscopic behavior does not depend on the specimen orientation.

4. Conclusion

Compressive creep behaviors of binary or ternary eutectics prepared from the Al_2O_3–Ln_2O_3–ZrO_2 phase diagram were studied in the temperature range 1400–1600 °C and stress range 70–200 MPa.The following conclusions were reached:

(1) The eutectics exhibit stress exponent values increasing with stress ($1 < n < 3$) for temperatures lower than 1500 °C and close to 3 for higher temperatures under any stress. These values ($n \geq 2$) indicate that dislocations play a role in deformation mechanisms.
(2) The eutectic compositions containing a garnet phase, at the difference of eutectic compositions containing a perovskite phase, display, at low stress (70 MPa), 2 deformation regimes with activation energies depending on temperature ($Q \sim 350\,kJ\,mol^{-1}$ at $T < 1500\,°C$ and $Q \sim 650\,kJ\,mol^{-1}$ at $T > 1500\,°C$). Only one regime is observed at higher stresses or temperatures for all the eutectics ($Q \sim 600\,kJ\,mol^{-1}$).
(3) The applied stress direction relatively to the crystallographic orientation of specimen does not really modify their creep behavior.
(4) Determination of operative slip systems from TEM studies has shown that the interconnected microstructure induces redistribution of applied stress, resulting in concentration of deformation in specific regions of microstructure. Local stresses are sufficiently high to activate pyramidal slip.
(5) Analyses of dislocation networks emphasize deformation by dislocation climb processes controlled by bulk diffusion.
(6) Alumina phase plays a major role in the first steps of plastic deformation of Al_2O_3–YAG composites (under low stress or temperatures lower than 1500 °C), with a dislocation density higher than those found in the garnet phase.
(7) Strain rates, stress exponents and activation energies of ternary eutectics are very similar to those of binary eutectics. However, their maximum strain (<5%) is lower than that of their binary counterparts ($\varepsilon_{max} \sim 10$ to 15%).

References

1. Hulse CO, Batt JA. The effect of eutectic microstructures on the mechanical properties of ceramic oxides. *Final Rept UARL-N910803-10, NTIS AD-781995/6GA* 1974.
2. Minford WJ, Bradt RC, Stubican VS. Crystallography and microstructure of directionally solidified oxide eutectics. *J Am Ceram Soc* 1979;**62**:154–7.
3. Sayir A, Farmer SC. The effect of the microstructure on mechanical properties of directionally solidified $Al_2O_3/ZrO_2(Y_2O_3)$ eutectic. *Acta Mater* 2000;**48**:4691–7.
4. Yi J, Argon AS, Sayir A. Creep resistance of the directionally solidified ceramic eutectic of $Al_2O_3/cZrO_2(Y_2O_3)$: experiments and models. *J Eur Ceram Soc* 2005;**25**:1201–14.
5. Llorca J, Orera VM. Directionally solidified eutectic ceramic oxides. *Prog Mater Sci* 2006;**51**:711–809.
6. Waku Y, Nakagawa N, Wakamoto T, Ohtsubo H, Shimizu K, Kohtoku YA. Ductile ceramic eutectic composite with high strength at 1873 K. *Nature* 1997;**389**:49–52.
7. Ochiai S, Ueda T, Sato K, Hojo M, Waku Y, Nakagawa N, et al. Deformation and fracture behavior of an Al_2O_3/YAG composite from room temperature to 2023. *Comp Sci Technol* 2001;**61**:2117–28.
8. Martinez-Fernandez J, Sayir A, Farmer SC. High-temperature creep deformation of directionally solidified $Al_2O_3/Er_3Al_5O_{12}$. *Acta Mater* 2003;**51**:1705–20.
9. Nakagawa N, Ohtsubo H, Mitani A, Shimizu K, Waku Y. High temperature strength and thermal stability for melt growth composite. *J Eur Ceram Soc* 2005;**25**:1251–7.
10. Pastor JY, Llorca J, Salazar A, Oliete PB, de Fransisco I, Pena JI. Mechanical properties of melt-grown alumina–yttrium aluminium garnet eutectics up to 1900 K. *J Am Ceram Soc* 2005;**88**:1488–95.
11. Hirano K. Application of eutectic composites to gas turbine system and fundamental fracture properties up to 1700 °C. *J Eur Ceram Soc* 2005;**25**:1191–9.
12. Waku Y, Sakata S, Mitani A, Shimizu K, Hasebe M. Temperature dependence of flexural strength and microstructure of $Al_2O_3/Y_3Al_5O_{12}/ZrO_2$ ternary melt growth composites. *J Mater Sci* 2002;**37**:2975–82.
13. Calderon-Moreno JM, Yoshimura M. Al_2O_3–$Y_3Al_5O_{12}$(YAG)–ZrO_2 ternary composite rapidly solidified from the eutectic melt. *J Eur Ceram Soc* 2005;**25**:1365–8.
14. Waku Y, Sakata S, Mitani A, Shimizu K, Ohtsuka A, Hasebe M. Microstructure and high-temperature strength of $Al_2O_3/Er_3Al_5O_{12}/ZrO_2$ ternary melt growth composite. *J Mater Sci* 2005;**40**:711–7.
15. Mazerolles L, Piquet N, Trichet MF, Parlier M. Microstructures and interfaces in melt growth Al_2O_3–Ln_2O_3 based eutectic composites. *Advances in science and technology*, vol. 45. Trans. Tech. Publications; 2006. p. 1377–1384.

16. Mazerolles L, Perrière L, Lartigue-Korinek S, Piquet N, Parlier M. Microstructures, crystallography of interfaces, and creep behavior of melt-growth composites. *J Eur Ceram Soc* 2008;**28**:2301–8.
17. Revcolevschi A, Dalhenne G, Michel D. External and internal interfaces of metal oxides. In: *Materials science forum.* Trans. Tech. Publications; 1988. p. 173–197.
18. Mazerolles L, Michel D, Hÿtch MJ. Microstructure and interfaces in directionally solidified oxide–oxide eutectics. *J Eur Ceram Soc* 2005;**25**:1389–95.
19. Ramirez-Rico J, Pinto-Gomez AR, Martinez-Fernandez J, de Arellano-Lopez AR, Oliete PB, Pena JI, et al. High-temperature plastic behaviour of Al_2O_3–$Y_3Al_5O_{12}$ directionally solidified eutectics. *Acta Mater* 2006;**54**:3107–16.
20. Snow JD, Heuer AH. Slip systems in α-Al_2O_3. *J Am Ceram Soc* 1973;**56**(3):153–7.
21. Heuer AH, Castaing J. Dislocations in α-Al_2O_3, advances in ceramics. In: Kingery WD, editor. *Structure and properties of MgO and Al_2O_3 ceramics*, vol. 10. The American Ceramic Society; 1984. p. 238–57.
22. Cadoz J, Castaing J, Phillips DS, Heuer AH, Mitchell TE. Work hardening and recovery in sapphire (α-Al_2O_3) undergoing prism plane deformation. *Acta Metall* 1982;**30**:2205–18.
23. Lagerloff KPD, Heuer AH, Castaing J, Rivière JP, Mitchell TE. Slip and twinning in sapphire (α-Al_2O_3). *J Am Ceram Soc* 1994;**77**(2): 385–97.
24. Heuer AH, Lagerloff KPD, Castaing J. Slip and twinning dislocations in sapphire (α-Al_2O_3). *Philos Mag A* 1998;**78**:747–63.
25. Castillo Rodriguez M, Castaing J, Munoz A, Veyssières P, Dominguez Rodriguez A. Analysis of a kink pair model applied to a mechanism in sapphire (α-Al_2O_3) deformed between 200 °C and 1800 °C. *J Am Ceram Soc* 2008;**91**(5):1612–7.
26. Karato S, Wang Z, Fujino K. High temperature creep of yttrium-aluminium garnet single crystals. *J Mater Sci* 1994;**29**:6458–62.
27. Corman GS. Creep of yttrium aluminium garnet single crystals. *J Mater Sci Lett* 1993;**12**:379–82.
28. Firestone RF, Heuer AH. Creep deformation of 0° sapphire. *J Am Ceram Soc* 1976;**59**(1–2):24–9.
29. Oishi Y, Kingery WD. Self diffusion of oxygen in single crystals and polycrystalline aluminium oxide. *J Chem Phys* 1960;**33**:480–6.
30. Prot D, Monty C. Self diffusion in α-Al_2O_3. II. Oxygen diffusion in undoped single crystals. *Philos Mag* 1996;**73**:899–917.